Applied Catalysis A, General 639 (2022) 118642

Contents lists available at ScienceDirect

Applied Catalysis A, General

journal homepage: www.elsevier.com/locate/apcata

Enhanced catalytic oxidation of diluted ethylene oxide on Pt/CeO_2 catalyst under low temperature

Yufeng Liu [a,b], Ying Zhou [a], Quanli Ke [a,*], Mei Lu [c], Wenxi Zhou [a], Guokai Cui [a], Xiaole Weng [d], Hanfeng Lu [a,*]

[a] Institute of Catalytic Reaction Engineering, College of Chemical Engineering, Zhejiang University of Technology, Hangzhou 310014, PR China
[b] Key Laboratory of Environmental Pollution Control Technology Research of Zhejiang Province, Eco-environmental Science Research & Design Institute of Zhejiang Province, Hangzhou, Zhejiang 310007, PR China
[c] Zhejiang Environmental Technology Co. Ltd., Hangzhou 311121, PR China
[d] Key Laboratory of Environment Remediation and Ecological Health, Ministry of Education, College of Environmental and Resource Sciences, Zhejiang University, Hangzhou 310058, PR China

ARTICLE INFO

Keywords:
Ethylene oxide
Diluted
Pt/CeO_2
Catalytic oxidation
Degradation pathway

ABSTRACT

A thorough catalytic combustion toward diluted ethylene oxide (EO) is demonstrated. The Pt active phase and CeO_2 support were selected to introduce a synergistic effect. As a result, a superior catalytic activity and less severe coking trend were observed on the Pt/CeO_2 catalyst when compared with another widely-used Pt/Al_2O_3 catalyst. The XPS spectra and H_2-TPR profiles evidenced that the Pt/CeO_2 catalyst has both stronger metal-support interaction and more abundant oxygen vacancies, which is believed at the heart of its excellent performance. Finally, the degradation pathways of EO were explored by *in-situ* DRIFTS. The weak H_2O affinity of Pt/CeO_2 catalyst can inhibit the polycondensation reaction and result in the favorable degradation of EO. In contrast, abundant hydroxyl species were present on the hydrophilic Pt/Al_2O_3 catalyst surface, which may serve as acid sites and complicate the EO degradation, and therefore various side products and carbon deposits would appear in this case.

1. Introduction

Ethylene oxide (EO), a new generation of excellent sterilant and disinfectant in succession to formaldehyde, is broadly used in the sterilization of medical industry due to its effectiveness and compatibility, especially in circumstances where the heat- or radiation-sensitive items are present (*e.g.* soft polymers) [1]. However, a certain amount of EO gas is remaining in the polymeric devices as well, which is not only flammable (Boiling point: 10.8 °C), but also significantly threatens both the environment and human health (WHO list of carcinogens, 2012, category I) [2]. To tackle this issue, a special ventilation process be adopted to completely remove the EO residual within the devices. Nonetheless, the resultant diluted EO waste would be another serious threat if exceeding permissible levels, for example, the permissible exposure limit for EO gas in the workplace is 1 ppm, while the limits for long-term (40 h per week, 8 h per shift) and short-term exposure (15 min) are 0.5 ppm and 5 ppm, respectively [2,3]. Therefore, the emission of diluted EO waste is now becoming an urgent issue to be addressed.

Conventionally, EO waste gas is eliminated by thermal oxidation, adsorption, and biodegradation. However, thermal catalysis generally requires a high operation temperature, which may cause EO explosion and thus safety problems [4]. Meanwhile, during the exothermic adsorption process, the concentrated EO gas may suffer from easy polymerization, which interferes with the recyclability of the adsorbents and complicates the EO treatment [5,6]. Finally, the EO abatement efficiency using biodegradation could be a problem in the real natural environment [7]. With these concerns, hydration of EO waste to produce ethylene glycol seems a more practical way. In this case, a series of acid catalysts, including ion-exchange resins, heteropolyacids, sulfonated silica gels, niobium oxide, layered niobic acid, and H-ZSM-5 zeolites, have been adopted to catalyze the EO waste hydration [8–14]. Nevertheless, the high infrastructure investments for the EO hydration process, *e.g.* the hydration reactor and distillation tower, make the process rather expensive in case of diluted EO exhaust treatment, and therefore a more efficient and economical elimination method is necessitated. Catalytic combustion is a promising method to efficiently and

* Corresponding authors.
E-mail addresses: quanlike@zjut.edu.cn (Q. Ke), luhf@zjut.edu.cn, lu.hanfeng@gmail.com (H. Lu).

https://doi.org/10.1016/j.apcata.2022.118642
Received 1 March 2022; Received in revised form 17 April 2022; Accepted 22 April 2022
Available online 26 April 2022

completely convert VOCs into harmless CO_2 and H_2O, while the milder operation temperature (than thermal oxidation) and lower investment (than hydration) could relieve the safety and economic concerns.

Catalysts are one of the most significant factors in catalytic combustion. Specifically, supported catalysts comprised of noble metal and redox-type support are proven to have particularly high activity toward oxygen-containing VOCs (OVOCs) under low temperatures. Among the noble metals, platinum-based catalysts have shown the most prominent performances. For example, Pt/TiO_2 effectively degrade formaldehyde and ethanol at room temperature, while Pt/CeO_2 decompose methanol completely at 60 °C [15–17]. In the meantime, a variety of OVOCs (*e.g.* isopropanol, acetaldehyde, butanone, and ethyl acetate) were proven to follow the MvK (Mars-van-Krevelen) mechanism during the catalytic oxidation process, *i.e.* OVOCs are adsorbed on the carrier surface and oxidized by the lattice oxygen, which stands out the significance for the migration and supplement of lattice oxygen within the support [18–22]. In this consideration, CeO_2 was an excellent candidate for catalyst support, as the conversion between Ce^{4+} and Ce^{3+} can promote the migration of its lattice oxygen and its redox activity [23,24]. Given this, it is strongly anticipated that the synergy between Pt particles and CeO_2 support could greatly enhance the EO oxidation efficiency, where EO is oxidized by the lattice oxygen on the CeO_2 surface and the consumed lattice oxygen is later recovered by the migrated oxygen species activated on the Pt particles (Scheme 1).

In this paper, Pt/CeO_2 catalyst was adopted in the catalytic oxidation of diluted EO sources, with concentrations as low as 3,000–10,000 ppm (0.3–1.0 vol%). The catalytic test results showed that Pt/CeO_2 has remarkably high catalytic activity for diluted EO sources under relatively low temperature. In contrast, when CeO_2 was replaced by another common support, Al_2O_3, both a higher conversion temperature and more severe coking tendency was observed on the Pt/Al_2O_3 catalyst, which stands out the better activity and stability of Pt/CeO_2 catalyst. The XPS spectra and H_2-TPR profiles proved that the stronger metal-support interaction and more abundant oxygen vacancies in Pt/CeO_2 catalyst were the key factors to its excellent performance. Finally, the different degradation pathways toward diluted EO source were given by *in situ* DRIFTs tests, and the degradation mechanism was proposed accordingly.

2. Experimental

2.1. Chemical and materials

Cerium nitrate hexahydrate (Macklin; 99.99%), Aluminum nitrate nonahydrate (SCR Co. Ltd; 99.9%), Zirconium nitrate pentahydrate (Macklin; 99.99%), Magnesium nitrate hexahydrate (SCR Co. Ltd; 99.0%), Zinc nitrate hexahydrate (SCR Co. Ltd; 99.0%), Manganese(II) nitrate aqueous solution (SCR Co. Ltd; 50.0%), Titanium oxysulfate-sulfuric acid hydrate synthesis grade (Aldrich; 93.0%), Hydrazine hydrate aqueous solution (SCR Co. Ltd; 85%), Ammonia aqueous solution (SCR Co. Ltd; 99.0%), (SCR Co. Ltd; 25.0–28.0%), Chloroplatinic acid hexahydrate (Shanghai Jiuyue Chemical Co. Ltd; 59.0%), Palladium chloride (Shanghai Chemical Co. Ltd; 59.0%), Tetrachloroauric acid tetrahydrate (SCR Co. Ltd; 47.8%). All chemicals of analytical grade were used as received without further purification.

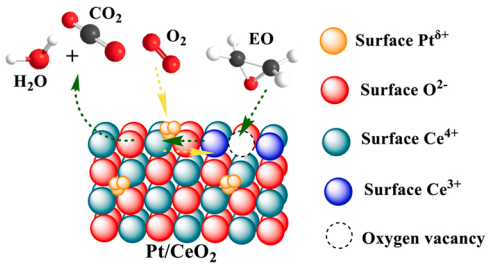

Scheme 1. The synergy between Pt particles and CeO_2 support in EO oxidation. **Green arrow:** the activation and oxidation of EO molecules on CeO_2 surface to consume lattice oxygen (Ce^{4+} to Ce^{3+}); **yellow arrow:** the supplement of consumed lattice oxygen (Ce^{3+} to Ce^{4+}) by the bond cleavage of oxygen molecules on Pt atoms and migration of activated oxygen species.

2.2. Catalyst preparation

2.2.1. Preparation of MOx

The MOx (M = Ce, Zr, Ti, Mn, Co, Zn, Mg, Al) supports are prepared by precipitation method with $NH_3{\cdot}H_2O$ as precipitant. Under vigorous stirring, ammonia solution was added dropwise into the cerium or aluminum nitrate solutions until the pH value was adjusted to 8–10. The mixture was then stirred for another 3 h, aged overnight, dried at 110 °C for 12 h, and finally calcined at 500 °C for 3 h.

2.2.2. Preparation of Pt/MOx

The desired amount of chloroplatinic acid solution (2.5 g_{Pt} / L) was first dissolved in 20 mL of deionized water. Then 1 g MOx powder was added into the chloroplatinic acid solution, and the resultant mixture was stirred at 75 °C water bath for 1 h. After filtration, the obtained solid was dissolved in another 20 mL of deionized water along with 140 μL of 85% hydrazine hydrate solution. The mixture above was reduced for 1 h and then filtrated, dried at 100 °C for 1 h, and finally calcined at 400 °C for 4 h. The obtained support catalysts were named as Pt/MOx (M = Ce, Zr, Ti, Mn, Co, Zn, Mg, Al), and the preparation method of N/CeO_2 (N = Pd, Au, Ag) is as above.

2.3. Catalyst characterizations

Physicochemical properties of the catalysts were characterized using a series of techniques, such as Chromatography-Mass Spectrometer (GC-MS), TG-DSC (Thermogravimetric Analysis-Differentials Canning Calorimetry), X-ray diffraction (XRD), Brunauer-Emmett-Teller (BET), Gas, X-ray photoelectron spectroscopy (XPS), and *in situ* Diffuse Reflectances Infrared Fourier Transform spectroscopy (*in situ* DRIFTs). The detailed characterization procedures can be seen from the Supplementary material.

2.4. Catalytic activity test

The performance of prepared materials in the oxidation of EO was investigated in a continuous-flow fixed-bed reactor at atmospheric pressure. In each test, 0.1 g of catalyst was placed into the tube reactor. The EO feed gas was generated by bubbling the EO liquid with air in an ice-water bath. The EO gas was then mixed with certain airflow (79% N_2 + 21% O_2) so that the total flow rate was maintained at 66.67 mL·min^{-1} (10,000 ppm EO and weight hourly space velocity = 40,000 mL/g·h). The catalyst bed was subsequently set to the desired temperature and left to equilibrium for 20 min before automatic sampling was initiated. In Fig. 1**A**, the sampling was initiated when each target temperature was reached and stabilized. In Fig. 1**B**, the sampling was performed immediately after the set temperature was reached, and the data were collected every 3 mins for in total ten times, as shown in Fig. S1.

The concentrations of EO were measured by gas chromatography (GC-1620; Jiedao, China) equipped with a flame ionization detector (FID) and RTX-1 column (30 m × 0.25 mm (ID) × 0.25 μm). The conversion of EO (X_{EO}) was calculated as follows:

$$X_{EO}\ (\%) = ([EO]_{in} - [EO]_{out}) / [EO]_{in} * 100\%$$

where $[EO]_{in}$ and $[EO]_{out}$ represent the EO concentrations in the inlet and outlet gas flows, respectively.

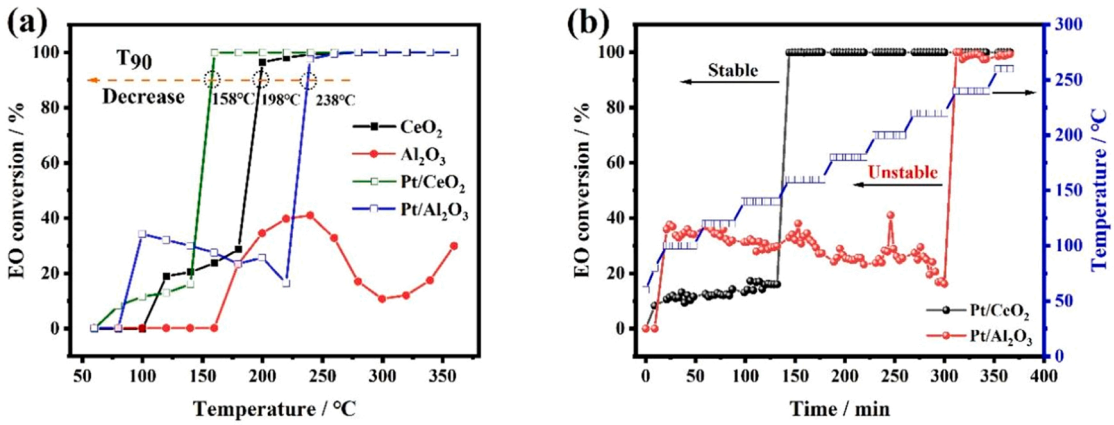

Fig. 1. (a) Light-off curves of CeO_2, Al_2O_3, Pt/CeO_2, and Pt/Al_2O_3; (b) Variation of EO conversion with the extended reaction time on Pt/CeO_2 and Pt/Al_2O_3 at different temperature. The inlet EO concentration was 10,000 ppm (or 1 vol%) and the weight hourly space velocity was kept at 40,000 mL/g·h. In Fig. 1**b**, the EO conversion data were first collected at 60 °C and 80 °C, and then the temperature was ramped up to 260 °C with 20 °C temperature interval. The EO conversion data were collected immediately after each target temperature was reached and the collection was kept for 30 mins each temperature (All the tests and data collection are repeated for three times and showed little deviations, as shown in Figs. S8 and S9).

3. Results and discussion

3.1. Catalyst activity evaluation

First, the catalytic oxidation performances for diluted EO gas were tested on the surface of different metal oxides, wherein CeO_2 showed the best catalytic activity, as witnessed by their full conversion temperatures for EO gas (Fig. S2). Thereafter, the same amounts of Pt (0.1 wt%) are further loaded on the surface of different metal oxides, and similarly, Pt/CeO_2 has the most excellent catalytic performance (Fig. S3). Basing on the results above, a series of noble metals were then loaded on CeO_2 support. In contrast to previous researches, Pt species, when serving as the active phase, exhibited obviously better catalytic oxidation activity for diluted EO stream when compared with other noble metals (Pd, Au, and Ag), as shown in Fig. S4 [25,26]. Provided the results above, the catalytic oxidation activity of Pt/CeO_2 and another widespread commercial catalyst, Pt/Al_2O_3, was then investigated by their light-off curves for 10,000 ppm (or 1 vol%) EO sources, with the performances on the sole supports (CeO_2 and Al_2O_3) as benchmark. A straightforward parameter for evaluating the catalyst activity be T_{90}, that is, the temperature at which 90% of the inlet EO mass was lost in catalytic combustion process. As shown in Fig. 1**a**, the EO catalytic oxidation performances on the oxide supports are obviously inferior to those catalysts with Pt loading (*e.g.* the T_{90} of CeO_2 decreases by 40 °C after Pt loading). Meanwhile, the T_{90} values of Pt/CeO_2 and Pt/Al_2O_3 are 158 °C and 238 °C, respectively, which proves the better cooperation between Pt species and CeO_2 support. Noticeably, the EO conversion on both the Pt/Al_2O_3 catalyst and Al_2O_3 support has exhibited decreasing trends during the catalytic oxidation (Fig. 1**a**), which were related to the temporary deactivation caused by the coverage of active sites [27]. This should also be the reason why their catalytic activity recovers again when the temperature increases to even higher degree. In order to verify the influence of noble metal loading, the catalytic performances of Pt/CeO_2 catalysts with different Pt loadings (0.1–0.4 wt%) were tested, whereas the increase of Pt loading only has slight influences on the EO catalytic oxidation activity (Fig. S5). Additionally, the catalytic oxidation tests were conducted for 3000–9000 ppm EO sources as well, the relatively lower T_{90} value of Pt/CeO_2 catalyst (Fig. S6), together with the results above, strongly verifies its excellent oxidation activity toward diluted EO.

To look deeper into the catalytic behavior of the catalysts, the change of EO conversion with time extension at each temperature was explored, as displayed in Fig. 1**b**. For the Pt/CeO_2 catalyst, the EO conversion came to equilibrium soon once the target temperature was reached, and increased immediately when the temperature rose to higher degree. On the contrary, the EO conversion over Pt/Al_2O_3 catalyst showed a trend of fluctuating downward within 30 mins, and this trend could be hardly reversed until the temperature reached 240 ℃. In order to check the reason for the decreased EO conversion during catalytic oxidation, the components within the outlet streams of both processes were analyzed at different conversion (T_{50}, T_{90}, and T_{100}) (Tables S1 and S2). As demonstrated, only a minor amount of acetic acid in addition to major CO_2 product (or minor EO resource) was observed in the outlet products when using Pt/CeO_2 as the catalyst; however, a considerable amount of acetaldehyde and/or acetic acid products were present in the outlet products till 90% EO conversion when Pt/Al_2O_3 was used instead (Fig. S7, Table S1). Previous research has also disclosed that acetaldehyde is one of the main products in EO degradation when using Al_2O_3 catalyst supported with noble metal [28–30]. As a result, the reaction kinetics and stability may also be varied by the different intermediates, since the intermediates, when adsorbed on the active sites, easily result in coke that interferes with the reaction between EO and active sites.

3.2. Carbon deposition analysis

Provided with the great influence of coke, the carbon deposits on the spent catalysts were then analyzed. First of all, the color change of the catalysts is the most direct reflection of the carbon deposition. According to Fig. 2**a**, the surface of the Al_2O_3 and Pt/Al_2O_3 catalysts obviously turned into darker colors when compared with those of CeO_2 and Pt/CeO_2. Thereafter, the thermogravimetric analyses of the spent catalysts were carried out to quantify the carbon deposit amount. Accordingly, three weight loss stages of the spent Pt/CeO_2 were witnessed. The first weight loss range (1.6 wt%, before 210 °C) could be attributed to the desorption of water, while the second (0.7 wt%, 210–300 °C) mainly to the catalytic oxidation of the chemically-adsorbed intermediates (*e.g.* residual acetic acid, more details in Section 3.4) adsorbed on the catalyst surface (Fig. 2**b**). Additionally, a very small weight loss can be observed in the third range (0.1 wt%, 300–350 °C), which reflects the minor coke formation on Pt/CeO_2 and fits well with the phenomenon in Fig. 2**a.**

As for the weight loss on the spent Pt/Al_2O_3 catalyst, a higher water desorption amount (3.8 wt%, before 170 °C) was found in the initial stage (Fig. 2**c**). Moreover, significantly greater weight losses were detected in the remaining two stages, which could be mainly associated with the catalytic oxidation of the chemically-adsorbed reaction intermediates (acetaldehyde, acetic acid or EO multimer, more details in Section 3.4) on the catalyst surface (5.0 wt%, 170–300 ℃), as well as the combustion of carbon deposits attached to the catalyst surface

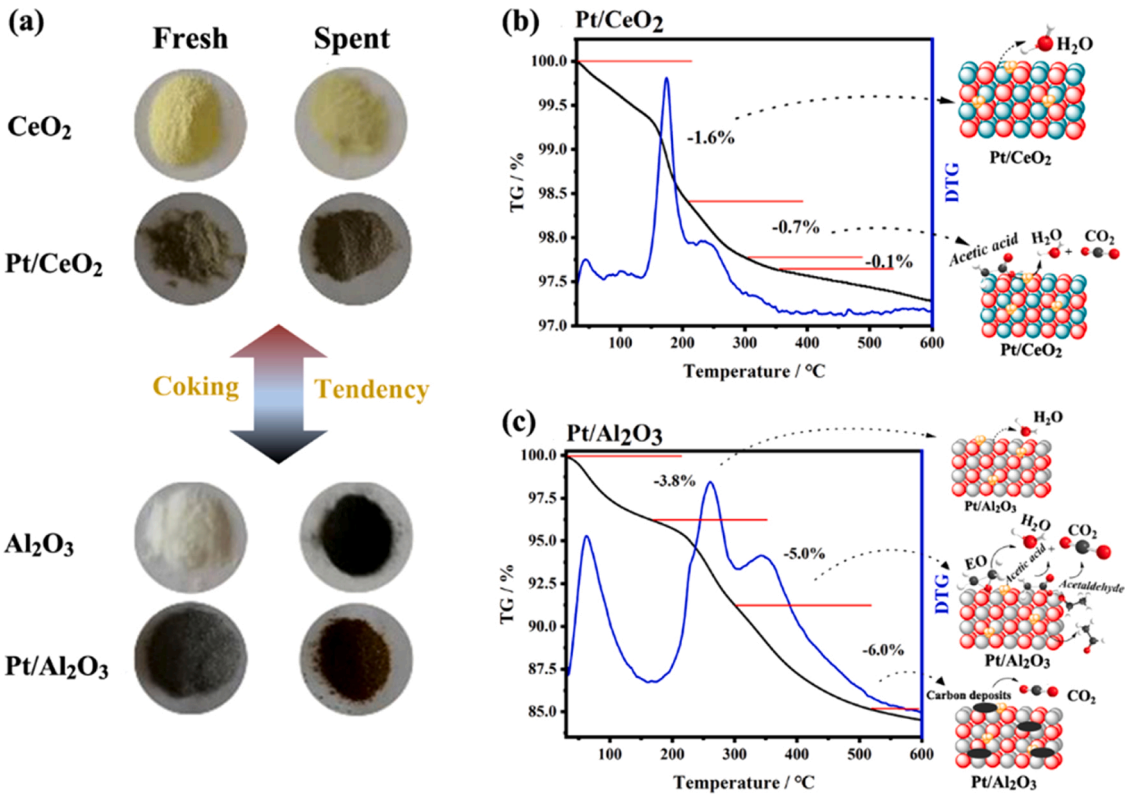

Fig. 2. (a) The appearance comparison of fresh and spent catalyst; (b) and (c) Thermogravimetric analyses of spent Pt/CeO_2 and Pt/Al_2O_3 catalysts. Both the Pt/CeO_2 and Pt/Al_2O_3 catalysts were held under 260 °C reaction before the TGA tests, which translates to full EO conversion on both catalysts according to Fig. 1. However, the reaction intermediates (acetaldehyde, acetic acid or EO multimer) are probably remaining in the catalysts.

(6.0 wt%, 300–520 ℃) (Fig. 2**c**). Previous researches have demonstrated that the surface acidity and porosity of catalysts were the most important factors for coke formation and proposed multiple reaction pathways of EO molecules on Al_2O_3 surface [31–33]. As a consequence, a variety of carbon deposits would be formed, which not only block the pores (shown in Fig. S10) but also cover the active sites and thus affect the catalytic activity of Pt/Al_2O_3. Nevertheless, even though Pt/CeO_2 has much smaller surface area, the EO gas could still be completely oxidized with little carbon deposition left and porosity changed (Fig. S11, Table 1). Thereby, it is rational to surmise that the Pt/CeO_2 catalyst surface recovered quickly for the next catalytic cycle, while the activation and migration of oxygen might play a fundamental role therein.

3.3. Characterization analysis

The O1s XPS spectra of the fresh and spent catalysts were then collected to investigate the role of oxygen in the catalytic oxidation reaction. Normally, there are two oxygen states on the solid surface. The first one is surface absorbed oxygen species which include the adsorbed oxygen (O^-, O^{2-}, O_2^-) and other oxygen species (*e.g.* water), while the second one is lattice oxygen [34–36]. As indicated in Fig. 3**a** and Table 1, the main peak at 528.9 eV was related to the lattice oxygen of cerium (O_{Latt}), while the weak peak at 531.3 eV to the surface absorbed oxygen (O_{Ads}). Meanwhile, the Ce 3d XPS spectra of CeO_2 support and Pt/CeO_2 catalyst are illustrated in Fig. S12, wherein two cerium states are present, *i.e.* Ce^{3+} and Ce^{4+}. The amount of Ce^{3+} is estimated to be 22.1% and 36.9% in CeO_2 support and Pt/CeO_2 catalyst, respectively. Notably, the high amounts of Ce^{3+} cations and abundant surface absorbed oxygen species on the Pt/CeO_2 catalyst surface strongly validates the presence of abundant surface oxygen vacancies, which also translates to a higher catalytic activity when participating in the EO catalytic oxidation [37]. Compared to Pt/CeO_2 catalyst (O_{Ads}: 27.3%), Pt/Al_2O_3 catalyst (O_{Ads}: 40.1%, Oxygen species: 20.8%) has a higher fraction of surface adsorbed oxygen species, mainly because of the presence of large amounts of hydroxyl groups and water on its surface (Fig. 3**b**, Table 1). This would promote the occurrence of various side reactions, as referred in literature previously [31–33]. After the reaction, the fractions of O_{Ads} and Oxygen species reach up to 44.6% and 26.9%, respectively, on the spent Pt/Al_2O_3 catalyst surface. This phenomenon could be attributed the remaining oxygen-containing intermediates, such as acetaldehyde, acetic acid and ethylene glycol. In contrast, only a small fraction of adsorbed oxygen assigned to the remaining oxygen-containing intermediates are witnessed on the Pt/CeO_2 catalyst surface, which proves

Table 1
the surface areas, H_2-TPR deconvolution and adsorbed oxygen ratios of fresh Pt/CeO_2 and Pt/Al_2O_3 catalysts.

Sample	S_{BET} (m^2/g)[a]	H_2-TPR		O_{Latt}/ (%)		O_{Ads}/ (%)		Oxygen species/ (%)	
		Peak position (℃)	H_2 consumption (μmol/g)[b]	Fresh	Spent	Fresh	Spent	Fresh	Spent
Pt/CeO_2	37.23	87, 384, 771	84.8, 146.0, 439.3	72.7	71.8	27.3	28.2	–	–
Pt/Al_2O_3	260.94	447	43.3	39.1	28.5	40.1	44.6	20.8	26.9

[a] The textual properties of all the samples were then obtained from the adsorption isotherms. The linearity of fitting for the Brunauer-Emmett-Teller (BET) specific surface area (SBET) was 0.99999.
[b] CuO is used as the standard material for the calculation of H_2 consumption, and the calculation processes were referred to the literature [43].

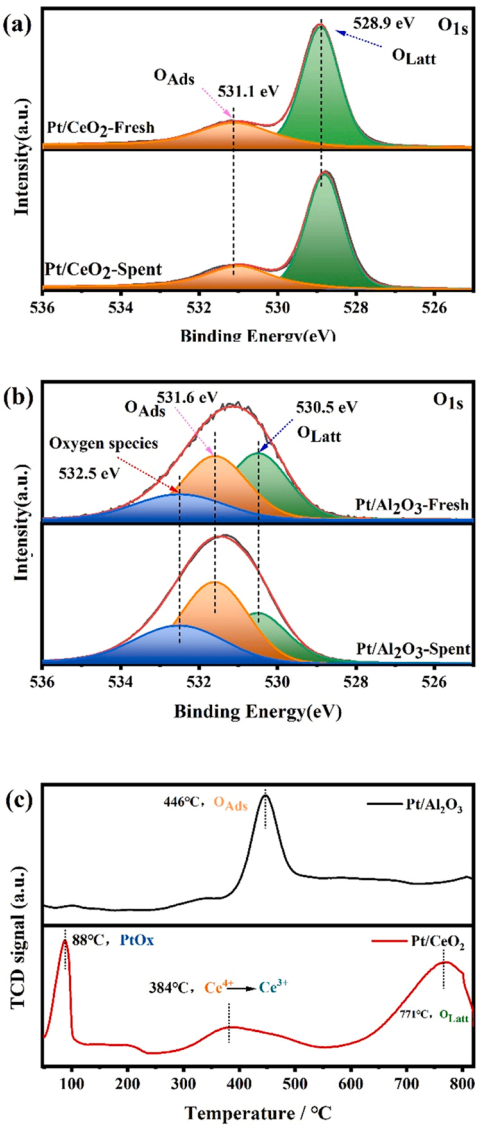

Fig. 3. XPS patterns of $O_{1\,s}$ of fresh and spent (a) Pt/CeO_2 and (b) Pt/Al_2O_3 catalyst; (c) H_2-TPR profiles of fresh Pt/CeO_2 and Pt/Al_2O_3 catalyst. In Fig. 3**a**, the orange, green, and blue area refer to adsorbed oxygen, lattice oxygen, and oxygen species, respectively. In Fig. 3**b**, the H_2 reduction peak for Pt/CeO_2 at 88 °C can be attributed to the reduction of PtOx species, the reduction peak at 384 °C corresponds to the transformation from Ce^{4+} to Ce^{3+} but away from the Pt particles, and the final reduction peak at 771 °C could be assigned to the reduction of the CeO_2 subsurface. Besides, the H_2 reduction peak for Pt/Al_2O_3 at 446 °C can be attributed to the reduction of surface oxygen species or PtOx species on Al_2O_3 surface. The reduction temperature of Al_2O_3 is out of the test range.

its stronger activation capability for the intermediates and therefore higher degradation efficiency for the EO molecules.

Subsequently, the surface reduction ability of the catalysts was investigated by H_2-TPR characterization. As shown in Fig. 3**c** and Table 1, Pt/CeO_2 has three reduction peaks at 88 °C, 384 °C, and 771 °C, respectively. The reduction peak at 88 °C can be attributed to the reduction of PtOx with an H_2 uptake of 84.8 μmol/g, which is significantly higher than the nominal value of 5.1 μmol/g (assuming that the Pt species in the catalyst is Pt^{2+}) [38]. The hydrogen spillover effect due to the metal-support interaction was responsible for the abnormally high H_2 uptake, including the contribution of surface oxygen adjacent to the Pt species. The second reduction peak at 384 °C corresponds to an H_2 consumption of 146 μmol/g, which caused by the reduction of surface oxygen away from Pt particles, so the transformation between Ce^{4+} and Ce^{3+} [39]. Finally, the reduction peak at 771 °C assigned to the oxygen reduction of the support subsurface, which corresponds to a H_2 consumption of 439.3 μmol/g. As a comparison, Pt/Al_2O_3 has only one H_2 reduction peak at 446 °C and the H_2 consumption is about 43.3 μmol/g (the reduction temperature of Al_2O_3 is out of the test range), which is higher than the nominal value of 5.1 μmol/g for Pt reduction (Table 1). This phenomenon ascribed to the reduction of surface oxygen species or weak metal-support interactions between Pt particles and Al_2O_3 [40]. However, it should also be noted that the H_2 consumption of Pt/Al_2O_3 is much lower than that of Pt/CeO_2 catalyst (84.8 μmol/g), which evidences the more advantageous electron transfer in the latter catalyst. In conclusion, H_2-TPR profiles and the XPS spectra prove that Pt/CeO_2 has shown stronger metal-support interaction (for oxygen activation) and more abundant oxygen vacancies (for EO activation) than Pt/Al_2O_3, which is the reason why Pt/CeO_2 exhibited better redox activity. That means, the Pt particles served as the active site for oxygen activation, while the oxygen vacancy in CeO_2 as the active sites for EO molecules. However, since the single CeO_2 support also shows quite good catalytic activity (Fig. 1), the O_2 molecules may also be effectively activated on CeO_2 surface [41,42].

3.4. Mechanism analysis

Since the GC-mass tests have verified diverse intermediates and implied different degradation pathways on the catalysts, *in situ* DRIFTs tests were then performed under the reaction conditions to track the reaction mechanism. Especially, information about the peak intensity change of different bonds is interesting as it directly reflects the evolution of reaction intermediates. At room temperature, only characteristic peaks associated with EO were observed on the Pt/CeO_2 surface: the first, the peaks at *ca.* 2761–3009 cm^{-1} and 1268 cm^{-1} are attributed to ν_{as}(C-H) stretching vibration and δ(C-H) bending vibration of methyl (-CH_3) and methylene (-CH_2) groups, respectively; besides, the peaks at *ca.* 1083 cm^{-1} and 867 cm^{-1} are assigned to the asymmetric ν_{as}(C–O–C) and symmetrical ν_s (C–O–C) stretching vibration of EO, correspondingly (Fig. S13) [44]. However, when the temperature increased to 80 ℃, a signal attributed to carbonyl (C═O) (*ca.* 1585 cm^{-1}) appeared and the peak intensity due to the C–H bond also increased (Fig. 4**a**), indicating the formation of acetaldehyde or acetic acid product [45]. As the temperature reached by 140 ℃, the characteristic peak intensity belonging to EO decreased, while another two stretching vibrations signals related to the aldehyde carbonyl group (C═O) (*ca.* 1693 cm^{-1}) and the carboxyl group (-COOH) (*ca.* 1369 cm^{-1}) were found to occur (Fig. 4**a**), which suggests the conversion of acetaldehyde into acetic acid [46,47]. When the temperature was further raised above 160 ℃, the signal ascribed to CO_2 species started to be detected (2285 cm^{-1}-2417 cm^{-1}), concurrently with the weakening of the aldehyde carbonyl group (C═O) (*ca.* 1693 cm^{-1}) and increasing of the carboxyl group (-COOH) (*ca.* 1369 cm^{-1}) (Fig. 4**a**, Fig. S14). The carboxyl group is considered to be derived from the acetic acid (evidenced by the GC-mass results), and thus the accumulation of acetic acid shows that the degradation of acetic acid may be the key step of EO catalytic oxidation on the Pt/CeO_2 surface. In the meantime, no obvious change was witnessed in the peak associated with hydroxyl species (3086 cm^{-1}-3357 cm^{-1}), indicating that the H_2O molecules generated by the reaction can easily depart from the catalyst surface (Fig. 4**a**). In the absence of H_2O molecules, the ring-opening polycondensation of EO would be inhibited, which well explains the remarkable anti-coking property of Pt/CeO_2 catalyst.

In contrast, a totally different band evolution was found on the surface of Pt/Al_2O_3 catalyst, as shown in Fig. 4**b**. At room temperature, the characteristic bands of EO were hardly observed (Fig. S13). When the temperature rose to above 80 °C, the characteristic band of CO_2 (*ca.* 2347 cm^{-1}) started to occur, and its intensity was found to increase until the temperature reached 120 °C (Fig. S15) [48]. This was caused by the formation of stable carbonate when the CO_2 accumulates on the catalyst

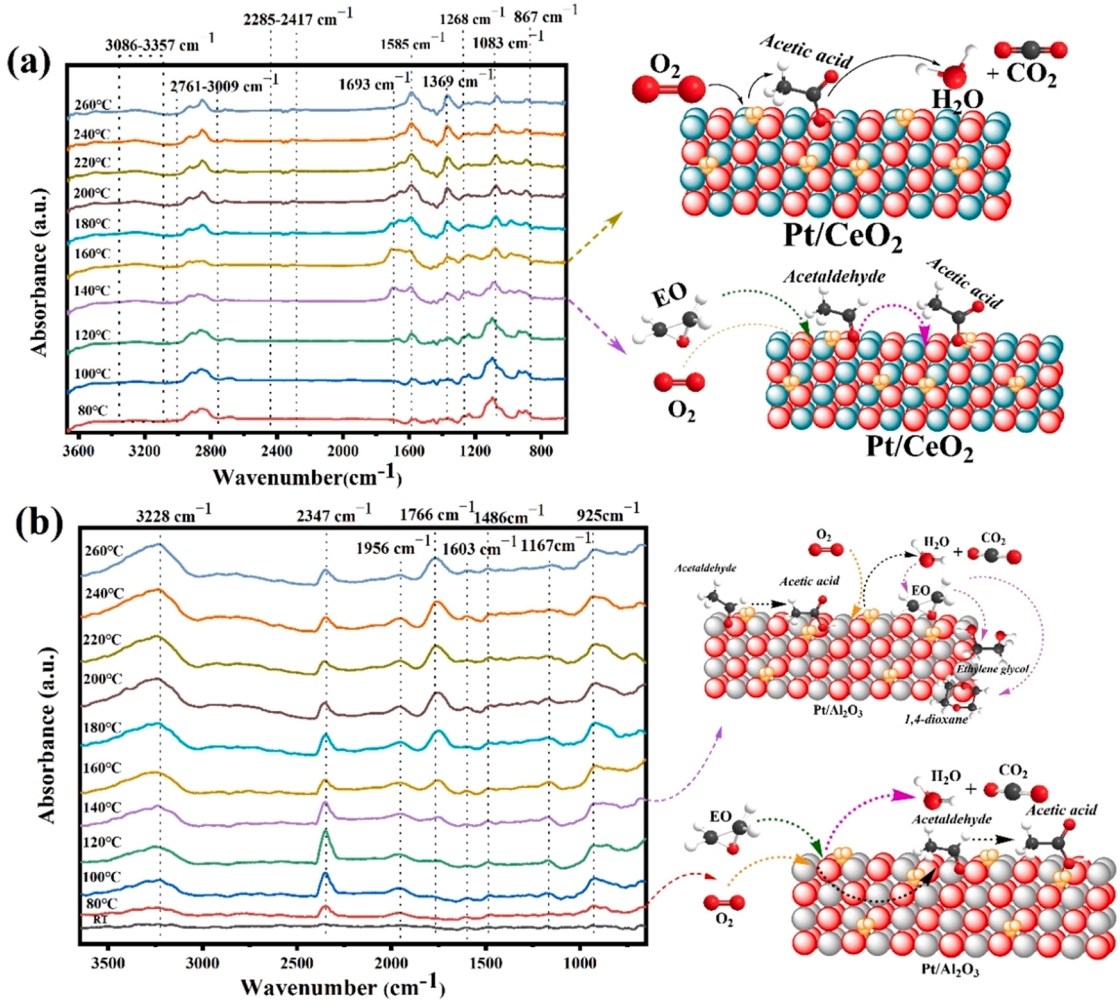

Fig. 4. *In situ* DRIFTs spectra of EO oxidation on (a) Pt/CeO_2 and (b) Pt/Al_2O_3 catalysts. The EO was injected with air at different temperatures. The inlet EO concentration was maintained at 10,000 ppm (or 1 vol%) and the weight hourly space velocity at 40,000 mL/g·h. In Fig. 4**a**, the signals related to carbonyl (C═O) vibration (*ca.* 1585 cm^{-1}), aldehyde carbonyl group (*ca.* 1693 cm^{-1}), carboxyl group (*ca.* 1369 cm^{-1}) and CO_2 vibration (2285 cm^{-1}-2417 cm^{-1}) are the most important ones. In Fig. 4**b**, three extra signals are also observed, which are assigned to the stretching vibration of the carboxylic carbonyl group (*ca.* 1766 cm^{-1}), the bending vibration of alcohol hydroxyl group (*ca.* 1486 cm^{-1}) and the C-O-C structure stretching vibration of the EO multimer (*ca.* 1167 cm^{-1}).

surface [49]. Notably, H_2O molecules, acetaldehyde and acetic acid were detected at the same time, as indicated by the signals at *ca.* 3228 cm^{-1}, 1956 cm^{-1}, 1603 cm^{-1}, and 925 cm^{-1}, which could be associated with the surface hydroxyl species, gaseous H_2O molecules, aldehyde carbonyl group and carboxyl hydroxyl group, respectively [44]. As the temperature continued to rise to higher than 120 °C, the characteristic band of CO_2 (*ca.* 2347 cm^{-1}) began to decrease, and three extra bands were observed [48]. The strong signal at *ca.* 1766 cm^{-1}, which is related to the stretching vibration of the carboxylic carbonyl group, was found to magnify continuously up to 260 °C. This phenomenon once again highlights the rate-determining role of the acetic acid degradation for EO catalytic oxidation on the Pt/Al_2O_3 surface, as is the case on the Pt/CeO_2 surface. Besides, the band at *ca.* 1486 cm^{-1} corresponds to the bending vibration of alcohol hydroxyl group, so the EO molecules may undergo a hydration reaction with H_2O on the catalyst surface to form ethylene glycol (EG) [33]. Additionally, the band at *ca.* 1167 cm^{-1} reflects the stretching vibration of the C-O-C structure in the EO multimer, either a dimer (1,4-dioxane) or a macromolecular polymer of EG molecules. These kinds of adsorbates are difficult to remove by catalytic combustion and easily form carbon deposits or even coke on catalyst surfaces [50]. Finally, as opposed to the Pt/CeO_2 catalyst, a strong and broadband attributed to the hydroxyl species (or acid sites) on the Pt/Al_2O_3 surface was always present within the whole temperature range, which should be originated from the reaction between H_2O and Al_2O_3 and would result in various side products and severe coking *via* acid catalysis (Fig. 2**a**, Fig. 4**b**). The stronger H_2O affinity of the Pt/Al_2O_3 catalyst was also evidenced by the catalytic activity tests with water vapor injection, where the activity of Pt/CeO_2 catalyst was maintained while that of Pt/Al_2O_3 catalyst deteriorate, both under 30% relative humidity condition (Figs. S16 and S17).

Based on the discussions above, the degradation pathways of EO on Pt/CeO_2 and Pt/Al_2O_3 are proposed, as shown in Scheme 2. On the surface of the Pt/CeO_2 catalyst, EO is first oxidized to form acetaldehyde and acetic acid, and finally leads to the fully-oxidized products of CO_2 and H_2O. Zhou et al. also showed that with the assistance of surface-active oxygen, CeO_2 can oxidize ethanol into acetaldehyde and acetic acid, and further into CO_2 and H_2O [51]. However, the degradation pathway of EO on the Pt/Al_2O_3 catalyst surface is more complicated. EO is initially fully oxidized to generate CO_2 and H_2O, which is similar to the case on Pt/CeO_2 surface. Subsequently, CO_2 accumulates on the catalyst surface and then stable carbonate species are formed. Nikawa *etc.* also observed stable carbonate ions, as the transition state, on the Au/TiO_2 catalyst surface due to the influence of Lewis acids and bases on the catalyst surface [20]. In this case, a higher temperature is required for CO_2 dissociation. Meanwhile, H_2O interacts with the surface of Al_2O_3 to generate a large number of hydroxyl species, which serve as acid sites

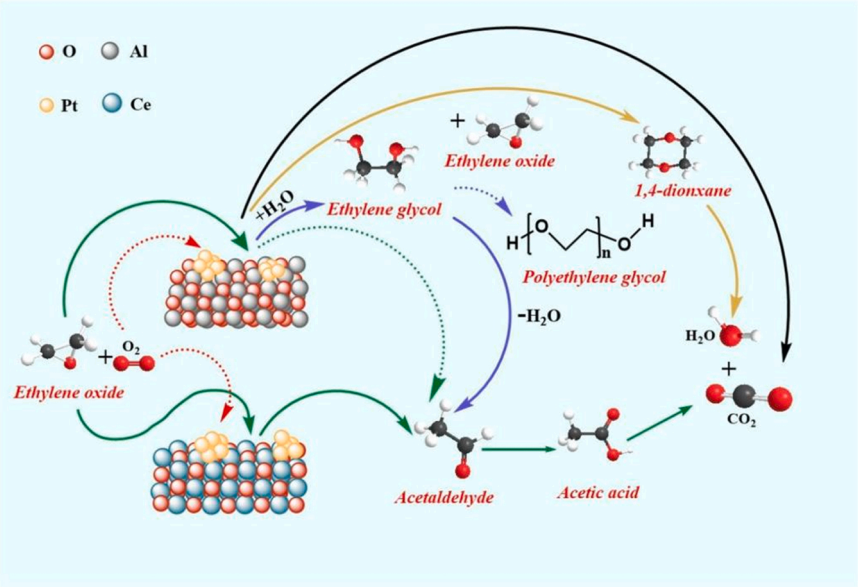

Scheme 2. Degradation pathway for EO catalytic oxidation over Pt/CeO_2 and Pt/Al_2O_3. The different intermediates are derived from the *in situ* DRIFTs spectra of EO oxidation on the catalysts together with the GC-mass tests of the outlet gases.

and result in a series of side products, such as EG and its derivatives [52]. Even though a part of EG molecules could still be fully oxidized, another part may undergo a polycondensation reaction to form dimer, polymer, or even coke and cover the active sites. The downward trends in the light-off curves of Al_2O_3 support and Pt/Al_2O_3 catalyst should also be caused by the coverage of the active sites (Fig. 1). Besides, Miller *etc.* proved as well that EO will undergo isomerization and hydration reactions on the Ag/Al_2O_3 catalyst surface to generate easily-polymerized side products (for instance, 1,4-dioxane) that are difficult to degrade [50]. In summary, a simple tandem degradation pathway was proposed on Pt/CeO_2, while multiple side reactions, as well as a more complicated degradation pathway, were observed on Pt/Al_2O_3, most likely due to the involved acid-catalyzed reactions.

4. Conclusions

As described, Pt/CeO_2 catalyst was employed in the catalytic oxidation of diluted EO sources and shown excellent catalytic activity and anti-coking property when compared with the widely-used Pt/Al_2O_3 catalyst as well as benchmark supports. The XPS spectra and H_2-TPR profiles proves that the prominent activity of Pt/CeO_2 catalyst is derived from its stronger metal-support interaction and more abundant oxygen vacancies. Finally, *in situ* DRIFTs tests were conducted under different temperature to investigate the different degradation pathways on the catalysts. A simple tandem degradation pathway, wherein EO was converted into acetaldehyde, acetic acid, and finally CO_2 and H_2O, was proposed on the Pt/CeO_2 catalyst. The polycondensation trend of EO on the Pt/CeO_2 catalyst was inhibited due to its weak H_2O affinity, which well explains its remarkable anti-coking property. On the contrary, a much more complicated degradation pathway was observed on Pt/Al_2O_3, possibly due to the concurrent acid catalysis processes on its surface that produced various side products. The high activity and weak H_2O affinity of Pt/CeO_2 catalyst make it quite promising in the practical conditions, and its scale-up applications could now be explored.

CRediT authorship contribution statement

Yufeng Liu: Investigation, Data curation, Writing – original draft. **Ying Zhou:** Formal analysis, Data curation, Writing – original draft. **Quanli Ke**: Supervision, Project administration, Writing – review & editing. **Mei Lu:** Resources, Formal analysis. **Wenxi Zhou:** Investigation, Data curation. **Guokai Cui:** Formal analysis, Funding acquisition. **Xiaole Weng:** Resources, Writing – review & editing. **Hanfeng Lu:** Conceptualization, Methodology, Funding acquisition.

Declaration of Competing Interest

We declare no conflict of interests.

Acknowledgments

This study was financially supported by Natural Science Foundation of China (No. 22078294), Zhejiang Provincial Natural Science Foundation of China (LZ21E080001, LGF20E080018), Key Laboratory of Environmental Pollution Control Technology Research of Zhejiang Province (No. 2021ZEKL04).

Appendix A. Supporting information

Supplementary data associated with this article can be found in the online version at doi:10.1016/j.apcata.2022.118642.

References

[1] H. Shintani, Biocontrol Sci. 22 (2017) 1–16, https://doi.org/10.4265/bio.22.1.
[2] L.S. Sreejith, R. Sasi, Trends Biomater. Artif. Organs 349 (2020) 7–12.
[3] G.C. Mendes, T.R. Brandão, C.L. Silva, Am. J. Infect. Control 35 (2007) 574–581, https://doi.org/10.1016/j.ajic.2006.10.014.
[4] W.N. Cheng, Chem. Ind. Technol. Dev. 10 (2013) 31–33 (in Chinese).
[5] X.L. Yang, Z.C. Zhang, CN 203507806 U. 2014.
[6] M.F. Lemanski, R. Kunin, US 6156942 A. 2000.
[7] J.W. van Hal, J.S. Ledford, X. Zhang, Catal. Today 123 (2007) 310–315, https://doi.org/10.1016/j.cattod.2007.02.015.
[8] J. Zhang, S.D. Liu, X.H. Pan, J. Zhao, X.Y. Zhao, CN 206473984 U. 2017.
[9] B. Beslin, H. Hasse, J. Plukhan, T. Maier, H. Auer, CN 1290837C. 2006.
[10] F. Wang, J. Chen, B. Zhang, Q. Chen, M. He, Chin. J. Catal. 26 (2005) 355–356 (in Chinese).
[11] Y. Li, S. Yan, L. Qian, W. Yang, Z. Xie, Q. Chen, B. Yue, H. He, J. Catal. 241 (2006) 173–179, https://doi.org/10.1016/j.jcat.2006.04.030.
[12] Y. Li, S. Yan, W. Yang, Z. Xie, Q. Chen, B. Yue, H. He, J. Mol. Catal. A-Chem. 226 (2005) 285–290, https://doi.org/10.1016/j.molcata.2004.10.047.
[13] Z.J. Yang, Y.F. Li, Q.B. Wu, N. Ren, Y.H. Zhang, Z.P. Liu, Y. Tang, J. Catal. 280 (2011) 247–254, https://doi.org/10.1016/j.jcat.2011.03.026.
[14] B. Sun, M. Wen, X. Ma, Y. Zhou, Q. Zhu, H. Lu, Environ. Technol. Innov. 15 (2019), 100376, https://doi.org/10.1016/j.eti.2019.100376.

[15] J. Chen, M. Jiang, W. Xu, J. Chen, Z. Hong, H. Jia, Appl. Catal. B 259 (2019), 118013, https://doi.org/10.1016/j.apcatb.2019.118013.
[16] Z. Jiang, M. Jing, X. Feng, J. Xiong, C. He, M. Douthwaite, L. Zheng, W. Song, J. Liu, Z. Qu, Appl. Catal. B 278 (2020), 119304, https://doi.org/10.1016/j.apcatb.2020.119304.
[17] V.P. Santos, S.A.C. Carabineiro, P.B. Tavares, M.F.R. Pereira, J.J.M. Órfão, J. L. Figueiredo, Appl. Catal. B 99 (2010) 198–205, https://doi.org/10.1016/j.apcatb.2010.06.020.
[18] J. Chen, D. Yan, Z. Xu, X. Chen, X. Chen, W. Xu, H. Jia, J. Chen, Environ. Sci. Technol. 52 (2018) 4728–4737, https://doi.org/10.1021/acs.est.7b06039.
[19] S.Y. Liu, S.M. Yang, Appl. Catal. A-Gen. 334 (2008) 92–99, https://doi.org/10.1016/j.apcata.2007.09.037.
[20] T. Nikawa, S.-i Naya, T. Kimura, H. Tada, J. Catal. 326 (2015) 9–14, https://doi.org/10.1016/j.jcat.2015.03.005.
[21] X. Liu, Q. Han, W. Shi, C. Zhang, E. Li, T. Zhu, J. Catal. 369 (2019) 482–492, https://doi.org/10.1016/j.jcat.2018.11.025.
[22] C. He, Z. Jiang, M. Ma, X. Zhang, M. Douthwaite, J.W. Shi, Z. Hao, ACS Catal. 8 (2018) 4213–4229, https://doi.org/10.1021/acscatal.7b04461.
[23] Z.L. Zheng, Carbon 108 (2016) 343–350, https://doi.org/10.1016/j.carbon.2016.07.040.
[24] K. Yuan, Y.W. Zhang, J. Chin. Rare Earth Soc. 38 (2020) 327–344 (in Chinese).
[25] H. Xu, Z. Zhang, J. Liu, C.L. Do-Thanh, H. Chen, S. Xu, Q. Lin, Y. Jiao, J. Wang, Y. Wang, Y. Chen, S. Dai, Nat. Commun. 11 (2020) 3908, https://doi.org/10.1038/s41467-020-17738-9.
[26] G.F. Zhou, J. Ma, S. Bai, L. Wang, Y. Guo, Rare Met. 39 (2020) 800–805, https://doi.org/10.1007/s12598-019-01347-7.
[27] Z. Hou, L. Dai, Y. Liu, J. Deng, L. Jing, W. Pei, R. Gao, Y. Feng, H. Dai, Appl. Catal. B 285 (2021), 119844, https://doi.org/10.1016/j.apcatb.2020.119844.
[28] C.J. Chen, J.W. Harris, A. Bhan, Chem. Eur. J. 24 (2018) 12405–12415, https://doi.org/10.1002/chem.201801356.
[29] J.E. van den Reijen, W.C. Versluis, S. Kanungo, M.F. d'Angelo, K.P. de Jong, P.E. de Jongh, Catal. Today 338 (2019) 31–39, https://doi.org/10.1016/j.cattod.2019.04.049.
[30] J.W. Harris, J.A. Herron, J.F. DeWilde, A. Bhan, J. Catal. 377 (2019) 378–388, https://doi.org/10.1016/j.jcat.2019.07.043.
[31] Y.S. Yong, E.M. Kennedy, N.W. Cant (Y), Appl. Catal. 76 (1991) 31–48, https://doi.org/10.1016/0166-9834(91)80003-F.
[32] D.A. Bulushev, E.A. Paukshtis, Y.N. Nogin, B.S. Bal'zhinimaev, Appl. Catal. A-Gen. 123 (1995) 301–322, https://doi.org/10.1016/0926-860X(94)00221-5.
[33] M. Casarin, D. Falcomer, A. Glisenti, A. Vittadini, Inorg. Chem. 42 (2003) 436–445, https://doi.org/10.1021/ic0257773.
[34] H. Zhang, S. Sui, X. Zheng, R. Cao, P. Zhang, Appl. Catal. B 257 (2019), 117878, https://doi.org/10.1016/j.apcatb.2019.117878.
[35] M. Wang, D. Chen, N. Li, Q. Xu, H. Li, J. He, J. Lu, ACS Appl. Mater. Interfaces 12 (2020) 13781–13789, https://doi.org/10.1021/acsami.9b20929.
[36] Q. Dai, S. Bai, Z. Wang, X. Wang, G. Lu, Appl. Catal. B 126 (2012) 64–75, https://doi.org/10.1016/j.apcatb.2012.07.008.
[37] J.M. López, A.L. Gilbank, T. García, B. Solsona, S. Agouram, L. Torrente-Murciano, Appl. Catal. B: Environ. 174–175 (2015) 403–412, https://doi.org/10.1016/j.apcatb.2015.03.017.
[38] H.H. Liu, Y. Wang, A.P. Jia, S.Y. Wang, M.F. Luo, J.Q. Lu, Appl. Surf. Sci. 314 (2014) 725–734, https://doi.org/10.1016/j.apsusc.2014.06.196.
[39] H. Huang, Q. Dai, X. Wang, Appl. Catal. B 158–159 (2014) 96–105, https://doi.org/10.1016/j.apcatb.2014.01.062.
[40] Q. Zhang, S. Mo, J. Li, Y. Sun, M. Zhang, P. Chen, M. Fu, J. Wu, L. Chen, D. Ye, Catal. Sci. Technol. 9 (2019) 4538–4551, https://doi.org/10.1039/C9CY00751B.
[41] M. Wang, X. Hong, J. Chen, J. Li, X. Chen, J. Mi, Z. Liu, S. Xiong, Chem. Eng. J. 440 (2022), 135854, https://doi.org/10.1016/j.cej.2022.135854.
[42] H. Wang, L. Wang, Q. Luo, J. Zhang, C. Wang, X. Ge, W. Zhang, F.-S. Xiao, Chem. Synth. 2 (2022) 2, https://doi.org/10.20517/cs.2022.02.
[43] P. Zimmer, A. Tschöpe, R. Birringer, J. Catal. 205 (2002) 339–345, https://doi.org/10.1006/jcat.2001.3461.
[44] S.F. Weng, Y.Z. Xu. Fourier Transform Infrared Spectroscopy, third ed., Chemical Industry,, Beijing, 2017.
[45] R. Zhang, D. Shi, N. Liu, Y. Cao, B. Chen, Appl. Catal. B 146 (2014) 79–93, https://doi.org/10.1016/j.apcatb.2013.03.028.
[46] Z. Jiang, M. Jing, X. Feng, J. Xiong, C. He, M. Douthwaite, L. Zheng, W. Song, J. Liu, Z. Qu, Appl. Catal. B 278 (2020), 119304, https://doi.org/10.1016/j.apcatb.2020.119304.
[47] X. Zou, Z. Rui, S. Song, H. Ji, J. Catal. 338 (2016) 192–201, https://doi.org/10.1016/j.jcat.2015.12.031.
[48] J. Chen, M. Jiang, J. Chen, W. Xu, H. Jia, J. Hazard. Mater. 392 (2020), 122511, https://doi.org/10.1016/j.jhazmat.2020.122511.
[49] B.B. Sarma, P.N. Plessow, G. Agostini, P. Concepción, N. Pfänder, L. Kang, F. R. Wang, F. Studt, G. Prieto, J. Am. Chem. Soc. 142 (2020) 14890–14902, https://doi.org/10.1021/jacs.0c03627.
[50] J.H. Miller, A. Joshi, X. Li, A. Bhan, J. Catal. 389 (2020) 714–720, https://doi.org/10.1016/j.jcat.2020.07.008.
[51] G. Zhou, B. Gui, H. Xie, F. Yang, Y. Chen, S. Chen, X. Zheng, J. Ind. Eng. Chem. 20 (2014) 160–165, https://doi.org/10.1016/j.jiec.2013.04.012.
[52] Y. Nosaka, A.Y. Nosaka, Chem. Rev. 117 (2017) 11302–11336, https://doi.org/10.1021/acs.chemrev.7b00161.